

Ultrafast Decay of the Excited Singlet States of Thioxanthone by Internal Conversion and Intersystem Crossing

Gonzalo Angulo,^[a] Jakob Grilj,^[c] Eric Vauthey,^[c] Luis Serrano-Andrés,^[b] Òscar Rubio-Pons,^[d] and Patrice Jacques^[e]

The experimental ultrafast photophysics of thioxanthone in several aprotic organic solvents at room temperature is presented, measured using femtosecond transient absorption together with high-level ab initio CASPT2 calculations of the singlet- and triplet-state manifolds in the gas phase, including computed state minima and conical intersections, transition energies, oscillator strengths, and spin-orbit coupling terms. The initially populated singlet $\pi\pi^*$ state is shown to decay through internal conversion and intersystem crossing processes via intermediate $n\pi^*$ singlet and triplet states, respectively.

Two easily accessible conical intersections explain the favorable internal conversion rates and low fluorescence quantum yields in nonpolar media. The presence of a singlet-triplet crossing near the singlet $\pi\pi^*$ minimum and the large spin-orbit coupling terms also rationalize the high intersystem crossing rates. A phenomenological kinetic scheme is proposed that accounts for the decrease in internal conversion and intersystem crossing (i.e. the very large experimental crescendo of the fluorescence quantum yield) with the increase of solvent polarity.

1. Introduction

Thioxanthone (TX; see Figure 1) photophysics is a prototype of the extreme dependence of photoinduced phenomena on the polarity and hydrogen-bonding properties of the environ-

(or regions) between either both states or via intermediate states. The degrees of freedom leading to the CI seam will be a protagonist of the vibronic coupling between the states.^[12]

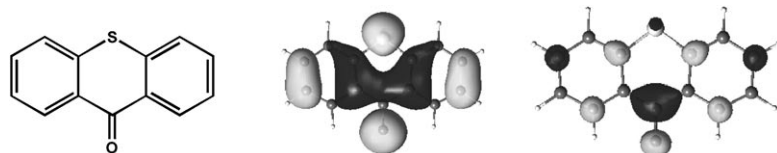


Figure 1. Structure of TX and representation of its HOMO and LUMO. CASSCF/ANO-L, $2^1A \pi\pi^*$ geometry.

ment.^[1-7] Large increases in the fluorescence quantum yield with the polarity have been reported previously, related to the concomitant decrease in the internal conversion (IC) rate from the excited spectroscopic state to the ground state. Although initially such a behavior was attributed to the “proximity effect”^[8] and subsequent vibronic coupling caused by the presence of close-lying $S_{\pi\pi^*}$ and $S_{n\pi^*}$ singlet states in polar environments, it is now well established that such a model, designed just considering the electronic states and their related energy gaps at the Franck-Condon (FC) region (ground-state geometry), is not generally applicable to explain ultrafast IC processes and fluorescence yield diminution.^[9] Modern photophysics and photochemistry understand IC processes as energy transfers taking place in regions of conical intersection (CI), that is, energy degeneracies between electronic states, typically displaying distorted molecular structures. The presence of such funnels is essential to explain the subpicosecond nature of most ICs.^[10-12] An ultrafast decay from $S_{\pi\pi^*}$ to the ground state requires evolution of the system toward a degeneracy region

Therefore, the decrease of the IC rates and increase of the fluorescence quantum yield in polar solvents for TX should be attributed to the fact that the corresponding CI or CIs are less accessible in such media.

The scheme is enriched by the known efficient population of the triplet manifold,^[10,13] which

[a] Dr. G. Angulo
Institute of Physical Chemistry
Polish Academy of Sciences, 01224 Warsaw (Poland)
Fax: (+48) 223433333
E-mail: gangulo@ichf.edu.pl

[b] Prof. L. Serrano-Andrés
Molecular Science Institute, University of Valencia
P.O. Box 22085, 46071 Valencia (Spain)
Fax: (+34) 963543274
E-mail: Luis.Serrano@uv.es

[c] J. Grilj, Prof. E. Vauthey
Department of Physical Chemistry, University of Geneva
1211 Geneva 4 (Switzerland)

[d] Dr. Ò. Rubio-Pons
Lehrstuhl für Theoretische Chemie, Technische Universität München
Lichtenbergstraße 4, 85747 Garching (Germany)

[e] Prof. P. Jacques
Department of Photochemistry
Université de Haute-Alsace, E.N.S.C.Mu
3 rue Alfred Werner, 68093 Mulhouse Cedex (France)

should also be initiated in a region of surface crossing and large spin-orbit coupling (SOC) between the initially activated singlet and the triplet states. The triplet quantum yield has also been established to be strongly solvent dependent.^[13] This richness makes TX an interesting candidate for studies of the interplay between crossing of the initial populated singlet state to the ground and triplet states. From a practical side, TX and its derivatives are widely used as photoinitiators of polymerization reactions, so the possible interferences and mechanisms in creation of the triplet state are relevant from this point of view.^[14] The solvatochromism of the molecule has been reported extensively,^[1,15,16] but until now no direct measurements of its excited-state dynamics have been performed in the very short time regime, which is the main focus herein. These measurements can reveal the mechanisms of deactivation of the singlet excited state and the relevance of the triplet-state population in such a process. For the sake of simplicity and due to the high sensitivity of TX to hydrogen bonding, which increases its fluorescence quantum yield,^[5,17] we have restricted our experimental study to solvents not showing specific interactions. High-level *ab initio* CASPT2 quantum-chemical calculations were also performed on the potential energy hypersurfaces and transition properties of the low-lying singlet and triplet excited states of TX to build a comprehensive model of its photophysics accounting for the reported measurements.

The article is organized as follows. We first describe the experimental details and the computational methods used. Then we present the experimental and theoretical results and the phenomenological kinetic scheme used to rationalize the data. Finally, in the discussion section we compare the theoretical and experimental results.

Experimental Section

TX was obtained from commercial sources and sublimated. The solvents cyclohexane (CX), *n*-dibutyl ether (DBE), tetrahydrofuran (THF), and acetonitrile (ACN) were provided by Aldrich and used without further purification. Steady-state absorption and fluorescence signals were recorded on a Cary 50 spectrophotometer and a Cary Eclipse fluorimeter, respectively.

The experimental setup for transient absorption has been described in detail earlier.^[18] Excitation was performed either at 400 nm by using the frequency-doubled output of a standard 1 kHz amplified Ti:sapphire system (Spectra-Physics) or at 490 nm with a home-built two-stage noncollinear optical parametric amplifier. The pump intensity on the sample was around 2 mJ cm⁻². The polarization of the probe pulses was at a magic angle relative to that of the pump pulses. The chirp of the white-light probe pulses was corrected following standard recipes.^[19] The zero time determination was done by following the Kerr effect signal of the solvent, with a precision similar to the time resolution of the apparatus, about 200 fs. The sample solutions were placed in a 1-mm-thick quartz cell, in which they were continuously stirred by N₂ bubbling. The optical density of the samples was adjusted to obtain a good signal-to-noise ratio in all experiments.

Computational Methods

Calculations were performed at the CASPT2//CASSCF(13/12), 13 electrons in 12 active molecular orbitals (MOs), level of theory.^[20] The active space includes the oxygen lone pair and 11 $\pi\pi^*$ electrons and MOs, and it was selected by careful analysis of the natural occupation numbers of the orbitals obtained in control restricted active space (RAS) self-consistent field (SCF) calculations.^[21,22] Geometries of singlet and triplet excited states were optimized at the CASSCF level maintaining the molecule plane with C_s symmetry. The final calculations were performed without spatial symmetry restrictions. The theoretical determination of different parameters was described earlier, such as the radiative lifetimes^[23] and the SOC terms,^[24,25] in all cases using CASSCF wave functions and CASPT2 energies. The core MOs and electrons were kept frozen in the CASPT2 calculations. An imaginary level-shift of 0.2 au was employed to prevent the presence of spurious intruder states.^[26] A one-electron basis set of atomic natural orbital ANO-L type contracted to S[5s4p2d]/C,O[4s3p1d]/H[2s1p]^[27] was used throughout the calculations, except for the determination of the CIs, which used a smaller basis set of the ANO-S type contracted to S[4s3p1d]/C,O[3s2p1d]/H[2s]. CIs were estimated without symmetry constraints as minimum-energy crossing points (MECPs) at the CASPT2 level using a grid of structures near the CASSCF-estimated MECPs.^[9] The MOLCAS suite of quantum-chemistry programs was employed throughout.^[28,29] The present methods and computational strategies have been shown in recent years to be the most accurate and balanced theoretical approaches to determine excited-state properties, and their performance has been firmly established.^[30–35]

2. Results and Discussion

2.1. Experimental and Theoretical Results

The main goal of the present study is to gain insight into the singlet excited-state deactivation process of TX, both in the gas phase and in solution. To this end, both theoretical *ab initio* calculations and experiments in different solvents of varying polarity (see Table 1) were performed. The sensitivity of the TX molecule to hydrogen bonding is well known,^[5,17] and this aspect, together with the eventual presence of water impurities in the media, has to be borne in mind when choosing the experimental strategy. For the sake of simplicity we will focus on the nonspecific interactions with the solvent, so none of the solvents used is a good H donor. As we have made use of a frequency-doubled Ti:sapphire laser excitation source, the near-UV position of the absorption spectra makes these measurements rather difficult due to the very low absorbance of TX at 390–400 nm. On the other hand, this red-edge excitation

Table 1. Some properties of the solvents used: dielectric constant ϵ , refractive index n_D , Kamlet–Taft parameters α , β , and π^* . ACN: acetonitrile, THF: tetrahydrofuran, DBE: *n*-dibutyl ether, CX: cyclohexane. Taken from ref. [36].

Solvent	ϵ	n_D	α	β	π^*
ACN	36.70	1.344	0.19	0.40	0.66
THF	7.73	1.407	0.00	0.55	0.55
DBE	3.08	1.397	0.00	0.46	0.18
CX	2.02	1.426	0.00	0.00	0.00

simplifies the results as it is known that only the $\pi\pi^*$ transition is excited at these wavelengths,^[15] and furthermore we avoid any vibrational cooling phenomena as the excess energy is close to zero.

Table 2 summarizes the CASPT2//CASSCF computed spectroscopic properties of isolated TX, and displays the lowest transitions in absorption and emission, including band origins, oscil-

State	Absorption/band maximum				Band origin			Vertical emission		
	ΔE [eV]	λ [nm]	f	μ [D]	ΔE (T_0) [eV]	λ [nm]	μ [D]	ΔE [eV]	λ [nm]	τ_{rad} [s]
1^1A	–	–	–	2.22	–	–	–	–	–	–
2^1A $n\pi^*$	3.49	355	0.000	0.80	3.22	385	0.64	2.48	500	1
3^1A $\pi\pi^*$	3.59	345	0.070	2.79	3.39	366	4.07	3.31	375	27×10^{-9}
1^3A $\pi\pi^*$	3.19	389	–	3.09	3.09	401	6.06	2.94	422	3
2^3A $n\pi^*$	3.32	373	–	0.63	3.20	387	0.73	2.50	496	28

lator strengths (f), state dipole moments (μ), and radiative lifetimes (τ_{rad}). The results compare well with the steady-state measurements. The most red absorption band of TX in solution at room temperature peaks around 375 nm (3.31 eV). The band consists of a superposition of two peaks that can be better distinguished in low-polarity solvents where the band width shrinks. The calculations assign these two transitions to the $n\pi^*$ and $\pi\pi^*$ excited states, respectively. Note that the $n\pi^*/\pi\pi^*$ state ordering changes after the excited state relaxes. In the presence of the reaction field of the solvent the effect is expected to be even larger, as the latter state has a larger dipole moment. The emission spectra are much more sensitive to the environment as the maximum goes from about 390 to 410 nm (3.18 and 3.02 eV) from CX to ACN, this being accompanied by band broadening. A description of the steady-state absorption solvatochromism of the molecule and its origin can also be found elsewhere.^[15]

Although computed vertical excitation energies at the ground-state optimized geometry can be reasonably well compared to absorption band maxima within the FC approach, we need calculations at the excited-state optimized geometries to compute band origins as the difference between the ground- and excited-state minima (T_0). It can be seen from Table 2 that both singlet states relax by about 0.2–0.3 eV. As expected, the basic geometric changes undergone by the states upon optimization are the elongation of the C=O bond length (more than 0.1 Å) for the $n\pi^*$ singlet and triplet states and the alternation of the single and double ring bonds for the $\pi\pi^*$ state. When compared with the bent ground-state structure, the dipole moment of the $\pi\pi^*$ state increases in the planar conformation. We also computed the vertical emission as the difference of energies from the excited-state minima and the ground state. It is common that at these geometries the FC approximation is not fulfilled as well as for absorption, and therefore the so-called vertical emission (just a theoretical concept) can be considered as a lower limit for the emission energy maximum. Finally, we obtained the radiative lifetime using the

Strickler–Berg approximation.^[23] As displayed in Table 2, these values point to the lowest $\pi\pi^*$ singlet excited state as the protagonist of both the absorption, computed from 3.6 to 3.4 eV in the isolated system, and emission, calculated from 3.4 to 3.3 eV. A more complete discussion of the photophysics of TX will be given later, based on both the experimental and theoretical findings. The latter include the state energy levels,

dipole moments, and transition properties at the optimized minima of the ground (S_0), $S_{\pi\pi^*}$, $S_{n\pi^*}$, and $T_{\pi\pi^*}$ lowest-lying singlet (S) and triplet (T) states, plus the calculation of two CIs: that connecting the $S_{\pi\pi^*}/S_{n\pi^*}$ states in a region intermedia between their minima, and the $S_0/S_{n\pi^*}$ CI, which leads to the final decay to the ground state. At low energies no CI has been found connecting the ground and $S_{\pi\pi^*}$

states, except for high-energy degeneracy regions in which the molecule splits (simultaneously breaking the C–C bonds fusing the side rings to the center moiety). It seems that the radiationless depopulation of the spectroscopic $S_{\pi\pi^*}$ state takes place via an intermediate state, in particular $S_{n\pi^*}$, as will be discussed later.

Figures 2 and 3 show the transient absorption (TA) spectra of TX in ACN and DBE, respectively. They consist of two bands, one at 700–750 nm (1.77–1.65 eV) and the other at 620–

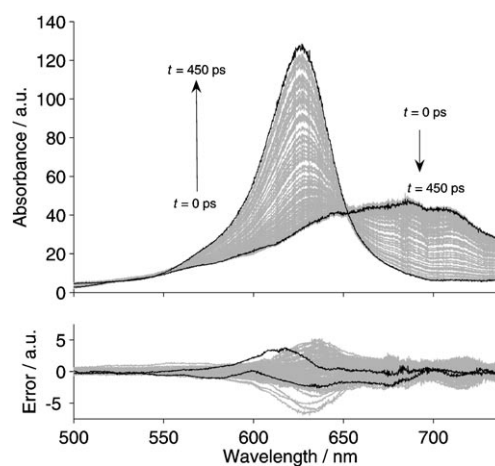


Figure 2. TA spectra measured with TX in ACN (top) and the difference between the experimental spectra and those obtained from the fit (bottom)—see text for details. The first and last spectra recorded are shown in black, and correspond roughly to the S–S absorption at short times and T–T absorption at long times.

650 nm (2.00–1.91 eV), as in all other solvents here studied, which can be ascribed to the S–S absorption and the T–T absorption, respectively, because the former disappears in the time range of picoseconds to tens of picoseconds and the latter stays for times much longer than the time limit of the

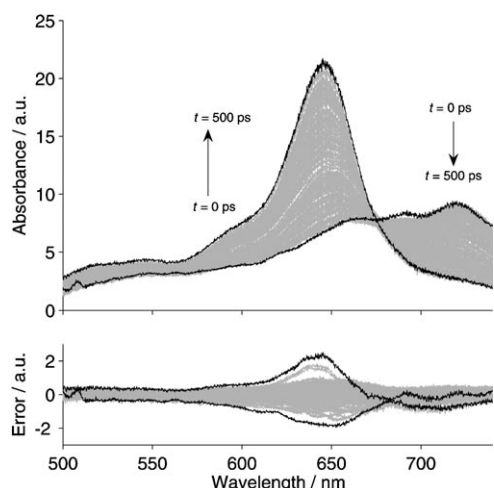


Figure 3. TA spectra measured with TX in DBE (top) and the difference between the experimental spectra and those obtained from the fit (bottom)—see text for details.

apparatus (2 ns). They are clearly kinetically bound, as indicated by the isobestic point also present in all the solvents. Another interesting observation is the hypsochromic shift of both bands with the solvent polarity, which indicates that the dipole moment of the absorbing states is higher than those to which they are promoted. These assignments are supported by the present theoretical results, as can be seen from the agreement with calculated transition energies and dipole moments. For this comparison we calculated TX properties at the singlet- and triplet-state optimized geometries.

Tables 3–5 show compilations of the excitation energies, oscillator strengths, and other properties of the low-lying excited states of TX computed at the CASPT2//CASSCF level at the geometry of the ground state, and the lowest relaxed singlet ex-

Table 3. Computed and experimental (CX) excitation energies (ΔE), wavelengths (λ), oscillator strengths (f), and dipole moments (μ) of TX (from ref. [15]).

State	Computed				Experimental	
	λ [nm]	ΔE [eV]	f	μ [D]	λ [nm]	ΔE [eV]
1^1A				2.22		
2^1A ($n\pi^*$)	355	3.49	0.000	0.80	377	3.29
3^1A ($\pi\pi^*$) ^[a]	345	3.59	0.070	2.79	362	3.43
4^1A ($\pi\pi^*$)	301	4.12	0.040	4.01	298	4.16
5^1A ($\pi\pi^*$)	275	4.51	0.140	3.51	287	4.32
6^1A ($\pi\pi^*$)	259	4.79	0.342	7.49	256	4.84
7^1A ($\pi\pi^*$)	248	5.00	0.012	1.30	247 sh	5.02
8^1A ($\pi\pi^*$)	240	5.17	0.112	7.44		
1^3A ($\pi\pi^*$)	389	3.19		3.08		
2^3A ($n\pi^*$) ^[a]	373	3.32		0.62		
3^3A ($\pi\pi^*$)	353	3.51		2.54		
4^3A ($\pi\pi^*$)	346	3.58		4.12		
5^3A ($\pi\pi^*$)	314	3.95		0.73		
6^3A ($\pi\pi^*$)	305	4.07		3.54		
7^3A ($\pi\pi^*$)	302	4.10		7.20		
8^3A ($\pi\pi^*$)	250	4.96		7.05		

[a] Computed with the largest SOC term ($3^3A \pi\pi^* - 2^3A n\pi^*$): 4.3 cm^{-1} .

Table 4. Computed CASPT2 singlet–singlet (S–S) excitations (ΔE_{S1}) [eV] and oscillator strengths (f_{S1}) of TX from the $2^1A \pi\pi^*$ singlet excited state at its optimized geometry, compared to the measured TA. State dipole moments (μ) and SOC [cm^{-1}] terms $2^1A \pi\pi^*$ –triplet state also included.

State	ΔE_{S1}	f_{S1}	μ [D]	Experimental ^[a]	SOC
1^1A	−3.31	0.1074	2.15	–	–
$2^1A \pi\pi^*$	–	–	4.06	–	–
$3^1A n\pi^*$	0.08	$< 10^{-8}$	0.99	–	–
$4^1A \pi\pi^*$	0.86	0.0127	3.73	–	–
$5^1A \pi\pi^*$	0.87	0.0002	2.48	–	–
$6^1A \pi\pi^*$	1.39	0.0094	3.21	–	–
$7^1A \pi\pi^*$	1.46	0.0122	2.11	–	–
$8^1A n\pi^*$	1.65	0.0001	1.25	–	–
$9^1A \pi\pi^*$	1.66	0.0063	3.11	–	–
$10^1A \pi\pi^*$	1.69	0.2511	4.11	1.77–1.65 eV 700–750 nm	–
$11^1A \pi\pi^*$	2.37	0.0008	2.51	–	–
$12^1A \pi\pi^*$	2.42	$< 10^{-8}$	1.13	–	–
$1^3A \pi\pi^*$	−0.25	–	4.36	–	< 0.01
$2^3A \pi\pi^*$	−0.19	–	1.18	–	< 0.01
$3^3A \pi\pi^*$	−0.18	–	2.23	–	< 0.01
$4^3A n\pi^*$	0.03	–	1.23	–	11.1
$5^3A \pi\pi^*$	0.43	–	2.40	–	< 0.01
$6^3A \pi\pi^*$	0.53	–	1.82	–	< 0.01
$7^3A \pi\pi^*$	0.76	–	2.62	–	< 0.01
$8^3A \pi\pi^*$	2.15	–	0.65	–	< 0.01

[a] TA spectra in ACN and DBE. See Figures 2 and 3.

Table 5. Computed CASPT2 triplet–triplet (T–T) excitations (ΔE_{T1}) [eV] and oscillator strengths (f_{T1}) of TX from the $1^3A \pi\pi^*$ triplet excited state at its optimized geometry, compared to the measured TA. State dipole moments (μ) are also included.

State	ΔE_{T1}	f_{T1}	μ [D]	Experimental ^[a]
1^1A	2.33	–	2.89	–
$1^3A \pi\pi^*$	–	–	0.94	–
$2^3A \pi\pi^*$	0.04	$< 10^{-9}$	0.70	–
$3^3A \pi\pi^*$	0.67	0.0017	3.10	–
$4^3A n\pi^*$	0.69	0.0036	5.69	–
$5^3A \pi\pi^*$	1.38	0.0104	3.91	–
$6^3A \pi\pi^*$	1.85	0.0113	0.56	2.00–1.91 eV 620–650 nm
$7^3A \pi\pi^*$	1.87	$< 10^{-5}$	2.44	–
$8^3A \pi\pi^*$	2.11	0.0025	2.46	–

[a] TA spectra in ACN and DBE. See Figures 2 and 3.

cited state ($2^1A \pi\pi^*$, $S_{\pi\pi^*}$) and triplet ($1^3A \pi\pi^*$, $T_{\pi\pi^*}$) excited states, respectively. The results in Tables 4 and 5 can be related to the TA S–S and T–T spectra, because they represent vertical absorptions from the lowest singlet and triplet excited-state minima, respectively. In particular, the peak ranging from 700 to 750 nm (1.77–1.65 eV) in the TA spectra can be assigned to the $2^1A \pi\pi^* \rightarrow 10^1A \pi\pi^*$ transition computed at 1.69 eV with the largest oscillator strength (f) in that region, and leading to a state with dipole moment (μ) similar to that of $S_{\pi\pi^*}$ (from the shift in the TA spectra a smaller value should, however, be expected). Equally the band observed at 620–650 nm (2.00–

1.91 eV) can be attributed to the $1^3A \pi\pi^* \rightarrow 6^3A \pi\pi^*$ transition computed at 1.85 eV with the largest f of all studied T–T promotions and leading to a state with half the value for μ than $T_{\pi\pi^*}$, as expected from the measured red shift upon lowering solvent polarity.

To analyze the time evolution of the TA, instead of choosing a wavelength or a spectral range, the whole spectra were analyzed at once as the bands are quite overlapped. Hence, the following matrix equation was applied [Eq. (1)]:

$$\mathbf{S}(\lambda, t) = \mathbf{C}(t) \times \mathbf{S}_c(\lambda) \quad (1)$$

where $\mathbf{S}(\lambda, t)$ are the full experimental spectra at each time t , $\mathbf{C}(t)$ the kinetics, and $\mathbf{S}_c(\lambda)$ the component spectra. $\mathbf{C}(t)$ values were obtained by solving the differential equations describing the reaction mechanisms tested. The rate constants entering these equations were the only fit parameters. Finally, $\mathbf{S}_c(\lambda)$ is the solution of the former matrix equation. The fit criterion was the difference between the reconstructed spectra and the experimental ones $\mathbf{S}(\lambda, t)$.

Several kinetic schemes of increasing complexity relating the lower singlet and triplet states were tried. The most robust results are compiled in Table 6. They were obtained following

Table 6. Results of fitting the scheme in Figure 4 to the experimental TA spectra. The free parameters are k_{TT} and k_{ISC} . k_F is taken from ref. [4] as $5.12 \times 10^{-5} \text{ ps}^{-1}$, and ϕ_T from ref. [13]. k_{IC} is calculated from the relationship held by the model $k_F + k_{IC} = (1/\phi_T - 1)k_{ISC}$. ϕ_F is the fluorescence quantum yield calculated from the obtained constants. $\phi_F(\text{calc})$ is calculated from the equation in ref. [4] that relates it to the solvent properties. All rate constants are given in ns^{-1} .				
	ACN	THF	DBE	CX
k_{TT}	$> 1 \times 10^3$			
k_{ISC}	8.0	63.5	107.8	182.6
k_{IC}	4.1	15.8	22.0	32.2
ϕ_T	0.66	0.8–0.85	0.8–0.85	0.85
ϕ_F	0.0042	0.0006	0.0004	0.0002
$\phi_F(\text{calc})$	0.0026	0.0007	0.0003	0.0002

the scheme displayed in Figure 4, which shows the states at the energy levels computed with CASPT2/CASSCF for the isolated molecule. Thus, the corresponding kinetic equations are [Eq. (2)]:

$$\begin{aligned} \frac{d[S_{\pi\pi^*}]}{dt} &= -(k_{IC} + k_F + k_{ISC})[S_{\pi\pi^*}] \\ \frac{d[T_{n\pi^*}]}{dt} &= k_{ISC}[S_{\pi\pi^*}] - k_{TT}[T_{n\pi^*}] \\ \frac{d[T_{\pi\pi^*}]}{dt} &= k_{TT}[T_{n\pi^*}] \end{aligned} \quad (2)$$

Additional reaction steps, such as a reversible intersystem crossing (ISC) between $S_{\pi\pi^*}$ and $T_{n\pi^*}$, did not lead to better re-

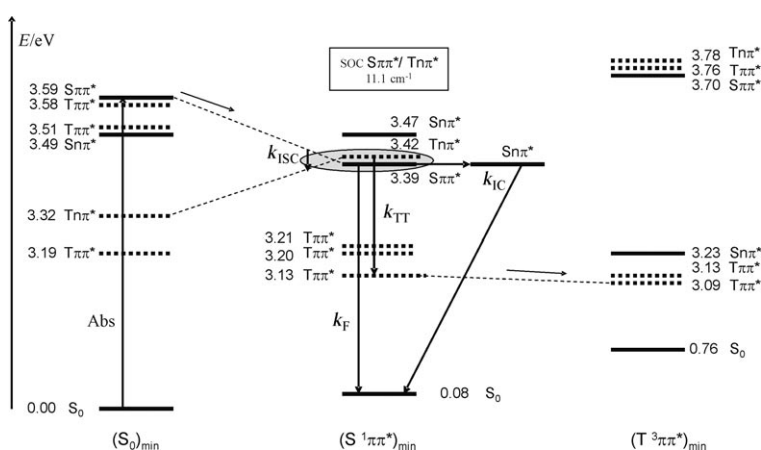


Figure 4. Scheme of the gas-phase photophysics of TX based on the CASPT2 calculations. All energies are relative to the ground-state energy at the FC, $(S_0)_{\text{min}}$, geometry. The most favorable region for ISC in the gas phase is shadowed and the computed SOC between the corresponding states is indicated. The experimental TA results have been analyzed in terms of the present reaction mechanism.

sults and did not yield unique solutions as they were extremely sensitive to the initial values. The data could be reproduced with a total error of about 10% (bottom panels in Figures 2 and 3). For the sake of coherence with the previous known properties of TX,^[16] the solutions of the differential equations have been restricted so that the final triplet quantum yield matches the known values (see Table 6). In addition, we made use of the fact that the radiative fluorescence rate constant is known to be insensitive to the solvent polarity, and equal to $5.12 \times 10^{-2} \text{ ns}^{-1}$.^[16] Small changes in the triplet quantum yield do not change appreciably the results obtained for the ISC and IC rate constants. For the TT rate constants we can only give approximate values, lower limits, as any large enough value compared to the other rate constants suffices to correctly reproduce the experimental results. The fluorescence quantum yields can be calculated from the obtained k_{IC} and k_{ISC} values. The results are in very good agreement with the yields obtained from the relationship with the Kamlet–Taft parameters found previously.^[16]

2.2. Discussion

Based on previous^[3,5,13,15,16] and present theoretical and experimental results we will now describe the photophysics of TX. As mentioned before, at the FC ground-state optimized geometry, $(S_0)_{\text{min}}$, the computed vertical excitation energies can be related to the absorption maxima in nonpolar solvents. Above 300 nm (below 4.12 eV) most of the initial energy will populate the lowest $S_{\pi\pi^*}$ singlet excited state, computed at 3.59 eV. This state is close in energy to the lowest $S_{n\pi^*}$ singlet state, at 3.49 eV (see Table 3). Their relative position was previously shown^[15] to be somewhat sensitive to the ground-state geometry, which easily breaks the planarity adopting a bent “butterfly”-like structure. As expected, the dark $S_{n\pi^*}$ and the somewhat brighter $S_{\pi\pi^*}$ states have dipole moments much smaller and larger, respectively, than that of the ground state, and subse-

quent blue and red shifts, also respectively, can be expected in polar (especially protic) solvents. In the absorption spectrum the two lowest-energy bands observed in nonpolar solvents get broader and move to lower energies on increasing the solvent polarity,^[15] an indication that it is the $S_{\pi\pi^*}$ state which carries most of the intensity.

To rationalize the photophysics of TX in different environments it is convenient to display an approximate scheme of the energy levels together with their dependence on the solvent polarity. To this end, we have projected the energies of the different states from the values in vacuum by using the Onsager reaction field theory [Eq. (3)].^[37]

$$E_S = E_v - \frac{2\mu^2}{4\pi\epsilon_0 a^3} \frac{\epsilon - 1}{2\epsilon + 1} \quad (3)$$

with $a = 3.53 \text{ \AA}$ obtained from the calculated AM1/QSAR van der Waals volume of the molecule, ϵ the dielectric constant of the environment, and μ the state electric dipole moment. This is a quite crude approximation, but good enough for a qualitative discussion of the trends observed on changing the solvent properties. Figure 5 displays the obtained results when using

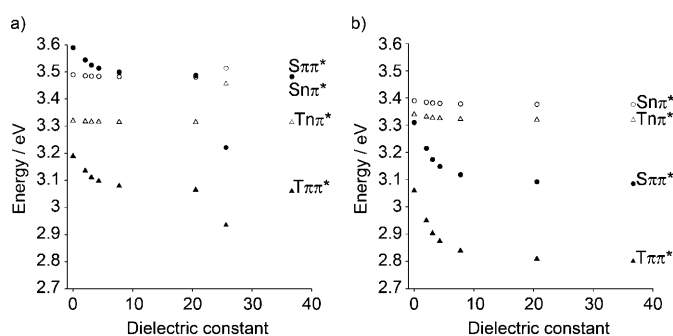


Figure 5. Energies of the four excited states involved in the IC and ISC processes with respect to the ground-state energy in vacuum, in solvents of different dielectric constants calculated from the values in vacuum at a) the FC geometry (Table 3) and b) $(S_{\pi\pi^*})_{\min}$ (Table 4). Equation (3) was employed.

the nonpolar energy levels computed at the S_0 (Table 3) and $S_{\pi\pi^*}$ (Table 4) optimized geometries, respectively. It can be seen that the $\pi\pi^*$ states are substantially influenced by the polarity of the environment whereas the $n\pi^*$ states are not, which leads to an approach of the $S_{\pi\pi^*}$ state to the $S_{n\pi^*}$ state at the FC geometry. For the equilibrium geometries of the $S_{\pi\pi^*}$ state, this stabilization is even more pronounced, placing both $\pi\pi^*$ states well below the $n\pi^*$ states.

Focusing first on the singlet manifold, the initially populated (at low energies) $S_{\pi\pi^*}$ state will subsequently relax toward equilibrium. Along the decay (see Figure 4) it is expected to cross with the close-lying $S_{n\pi^*}$ state, which is at higher energy than the former for the $S_{\pi\pi^*}$ geometry (middle of Figure 4). As illustrated in Figure 5, in more polar environments the interaction of both states can take place immediately because of the stabilization of the $S_{\pi\pi^*}$ state, which has a dipole moment (2.79 D) larger than that of the ground state (2.22 D), a difference that

increases at the $S_{\pi\pi^*}$ -state minimum. This initial $S_{\pi\pi^*}/S_{n\pi^*}$ crossing can be the source of a secondary decay pathway via the $S_{n\pi^*}$ state, especially in low-polarity environments. As shown later the $S_{n\pi^*}$ state has an open channel for radiationless relaxation to the ground state via the $(S_0/S_{n\pi^*})_{CI}$. In any case, most of the population that continues in the singlet manifold remains at the $S_{\pi\pi^*}$ state, which, independently of the solvent, can also be considered as the source of the fluorescence. In fact, using the data for ACN ($\phi_F = 0.0041$ and $\tau_F = 0.07 \text{ ns}$),^[4,5] a radiative lifetime ($\tau_{\text{rad}} = \tau_F/\phi_F$) of 17 ns is obtained for the emitting state, in very good correspondence with our computed value of 27 ns for the $S_{\pi\pi^*}$ state. Its dipole moment, which is near 1–2 D larger than that of the ground state, explains the observed red shift in the emission spectrum. The fluorescence quantum yield also increases when increasing the solvent polarity, in ACN being one order of magnitude larger than in the less polar THF.^[5] As clearly illustrated in Figure 6b, the stabilization of the $S_{\pi\pi^*}$ state in the more polar solvents can be expected to favor the fluorescence emission, the quantum yield of which increases by three orders of magnitude on going from THF to ethylene glycol.^[4,5] The decay toward the ground state is clearly less favorable in polar solvents because the deactivation path through the final $(gs/n\pi^*)_{CI}$ becomes less accessible due to the increase of the energy barriers.

To explain the nonadiabatic decay of the initially populated $S_{\pi\pi^*}$ state, it is necessary to determine the presence of the funnels leading to the population switch. So far, our model for TX in the gas phase indicates that the activated system favorably reaches the $S_{\pi\pi^*}$ -state minimum. From there, and apart from the ISC transfer to the triplet manifold that will be discussed later, the system might produce fluorescence or continue the population transfer to another state if an accessible CI exists. As mentioned before, the theoretical search for a CI between the $S_{\pi\pi^*}$ state and the ground state at low energies was unsuccessful. The $S_{\pi\pi^*}$ state can be basically described as an electron promotion from the highest occupied MO (HOMO) to the lowest unoccupied MO (LUMO) in TX.^[15] As shown in Figure 1, the HOMO has a bonding character for the C–C bonds parallel to the short molecular axis and for the bonds linking the side rings to the central moiety. Upon promotion to the LUMO (see Figure 1), a clear antibonding (or nonbonding) nature is displayed for the same C–C bonds and also for the C=O bond. The only CI found connecting the ground and $S_{\pi\pi^*}$ states is too high in energy and represents the breaking of the mentioned C–C bonds and the splitting of the molecule (with two channels, one for each of the side rings). In such a case the molecule remains planar, a situation extremely favored in the $S_{\pi\pi^*}$ state. The absence of a low-energy accessible $S_0/S_{\pi\pi^*}$ CI seam is an indication that the $S_{\pi\pi^*}$ state does not decay directly to the ground state. We have found, however, an $S_{\pi\pi^*}/S_{n\pi^*}$ CI placed just 0.06 eV (3.45 eV adiabatically from the FC ground state) higher in energy than the $S_{\pi\pi^*}$ minimum with a structure that it is intermediate between those of the $S_{\pi\pi^*}$ and $S_{n\pi^*}$ minima. For instance, the C=O bond length is 1.31 Å at the CI whereas it is 1.27 and 1.36 Å, respectively, in the other structures. Therefore, in the gas phase (or in nonpolar environments) the system can be expected to easily switch from the $S_{\pi\pi^*}$ mini-

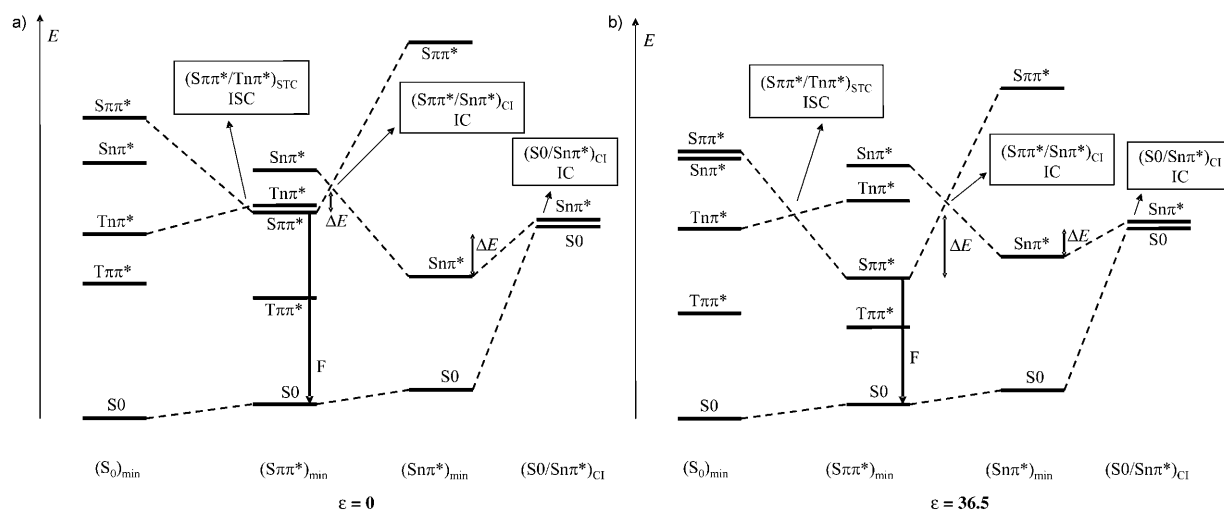


Figure 6. Qualitative scheme of energy levels, based on the CASPT2 and CASPT2 plus Onsager model (see Figure 4) results, for the most important low-lying singlet and triplet states of TX in the absence (a) and presence (b) of an external polar environment. Four geometries, the ground S_0 , $S_{\pi\pi^*}$, and $S_{n\pi^*}$ states minima, and the $S_0/S_{n\pi^*}$ CI are used. The ISC process takes place earlier along the $S_{\pi\pi^*}$ relaxation path in polar solvents. Energy barriers for IC processes (ΔE , double arrows) are largely affected by polarity.

imum toward the $S_{n\pi^*}$ state, therefore decreasing the probability of emission and the fluorescence quantum yield, and displaying a short lifetime.

Once on the $S_{n\pi^*}$ hypersurface, the system can evolve toward the state minimum (placed 0.23 eV below the previous CI) or toward a new funnel connecting the $S_{n\pi^*}$ and the ground state through the $S_0/S_{n\pi^*}$ CI seam. We have computed this structure as lying adiabatically at 3.36 eV, that is, 0.14 eV above the $S_{n\pi^*}$ minimum. The $S_0/S_{n\pi^*}$ CI lies 0.09 eV below the $(S_{\pi\pi^*}/S_{n\pi^*})_{CI}$ in the gas phase, where the system has therefore enough excess energy to surmount the barrier and decay to the ground state in an ultrafast manner. The $S_0/S_{n\pi^*}$ CI represents a distorted structure in which the C=O bond has enlarged up to 1.58 Å and the molecule has broken the planarity, thus leading to a “butterfly”-like conformation with a dihedral angle of 22°.

The presence at low energies of the two described CIs, $(S_{\pi\pi^*}/S_{n\pi^*})_{CI}$ and $(S_0/S_{n\pi^*})_{CI}$, puts forward a model to describe the decay of excited TX in the singlet manifold consisting of two successive IC processes. In the gas phase, the initially populated $S_{\pi\pi^*}$ state may easily relax to equilibrium and from there access the $(S_{\pi\pi^*}/S_{n\pi^*})_{CI}$ placed just 0.06 eV (1.4 kcal mol⁻¹) higher in energy. This population switch toward the $S_{n\pi^*}$ state may quickly continue toward the next funnel, $(S_0/S_{n\pi^*})_{CI}$, which lies slightly lower in energy than the previous one and finally brings the system to the ground state. The accessibility of both CIs in the gas phase and nonpolar media explains the measured low fluorescence quantum yields in such solvents, for instance, 6.2×10^{-4} in THF.^[5] Upon increasing the solvent polarity, both the fluorescence intrinsic lifetimes and quantum yields increase, an indication that the deactivation channels are less accessible. Indeed, because of its large dipole moment (4.07 D), the $S_{\pi\pi^*}$ -state minimum will be strongly stabilized in polar solvents with respect to any other situation, in particular the $(S_{\pi\pi^*}/S_{n\pi^*})_{CI}$, where the state has a dipole moment of

2.41 D. The barrier for deactivation from $(S_{\pi\pi^*})_{min}$ will therefore largely increase in polar media. Regarding the fate of the path via the $S_{n\pi^*}$ state in solution, the computed dipole moments can help us to predict the change in energy barriers. Whereas the $S_{n\pi^*}$ state in its minimum has a dipole moment of 0.64 D, this value increases more than 1 D at the $(S_0/S_{n\pi^*})_{CI}$ structure. It is expected that the barrier from the state minimum to the CI computed for the isolated system largely decreases, because the state will destabilize much more at its minimum in polar solvents. Figure 6 contains a qualitative scheme of the photo-physics of TX in both nonpolar and polar environments based on the present results. The location of the CIs leading to the main IC processes is indicated.

Apart from the decay via the singlet states, the population of the triplet manifold through an ISC process is known to be quite efficient in TX (see Table 6). We should analyze how the $S_{\pi\pi^*}$ state deactivates toward the triplet states. For the ISC to take place in an ultrafast manner, two requirements must be approximately fulfilled simultaneously: an energetically accessible singlet–triplet crossing should be reached and the corresponding SOC terms between the states should be large enough.^[10,25,38] The coupling of the initially populated (at low energies) $S_{\pi\pi^*}$ state (computed at 3.59 eV in the isolated system) with the triplet states near the FC geometry is less likely in the gas phase. In accordance with the qualitative El-Sayed rules,^[39] our computed SOC terms between $S_{\pi\pi^*}$ and the other close-lying $T_{\pi\pi^*}$ states (see Figure 4, right) are extremely low (< 0.01 cm⁻¹), whereas, even if the SOC term is higher with the closest $T_{n\pi^*}$ state (4.3 cm⁻¹), this is placed too far in energy (at 0.27 eV) from $S_{\pi\pi^*}$. In polar solvents, the gap $S_{\pi\pi^*}/T_{n\pi^*}$ is expected to be still large (0.2 eV, see Figure 5) at the FC region. Upon geometrical relaxation of $S_{\pi\pi^*}$ toward its minimum a crossing with the $T_{n\pi^*}$ state will take place (see Figure 4). Figure 6 shows the energy levels in TX in the absence and presence of polar environments that may help one to under-

stand the mechanism. It is worth mentioning that the electronic SOC terms computed here may largely increase if vibrational effects are considered, particularly those corresponding to out-of-plane modes, as proven by the calculations of Marian and co-workers^[40,41] on ISC rates in systems of similar size. The electronic values obtained here are, however, adequate for the present purpose of identifying the regions of the hypersurface simultaneously displaying small singlet–triplet gaps and large SOC terms.

Figure 7 displays the rate constants for the IC (singlet) and ISC processes from $S_{\pi\pi^*}$ to S_0 and $T_{n\pi^*}$, respectively, represented as a function of the respective state energy differences (ac-

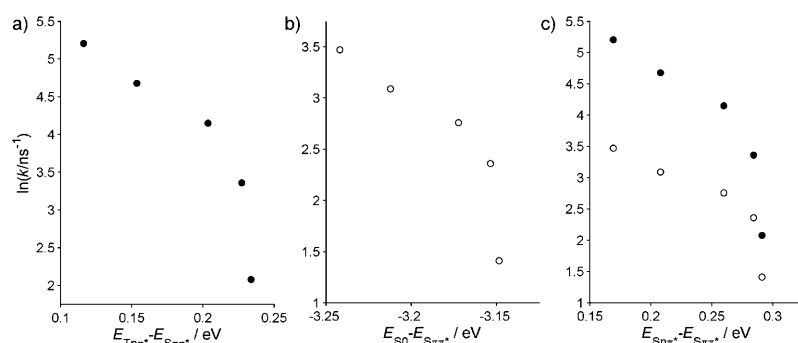


Figure 7. Rate constants of ISC (a) and IC (b) obtained by fitting the kinetic equations corresponding to the scheme of Figure 4 to the TA signals of TX in different solvents, as a function of the corresponding transition energy differences taken from the values in Figure 5. The plot in (c) compares the former rates (point codes are in correspondence with the other two plots) as a function of the energy difference between the two lowest singlet states.

ording to the change in polarity seen in Figure 5). A clear linear trend is seen in both cases, with similar slopes. As also inferred from the TA spectra, increasing the solvent polarity decreases both the rate of conversion of singlet into triplet states and the IC to the ground state. The linear trend might indicate a relative insensitivity of the SOC to the energy difference between the singlet and triplet states, or that another factor controls the dependence on the solvent polarity. According to the previous data (see Figure 6), the ISC process in polar solvents would take place closer to the FC region, whereas in nonpolar environments the favorable crossing would occur near the $S_{\pi\pi^*}$ -state minimum. The plots of these rate constants against the energy differences with respect to $S_{\pi\pi^*}$, while behaving linearly at lower polarities, show sudden drops at high polarities. This behavior is surely related to the large stabilization of the $S_{\pi\pi^*}$ state and the destabilization of the $S_{n\pi^*}$ and $T_{n\pi^*}$ states in polar solvents. For the singlet IC rate, closer $S_{\pi\pi^*}$ and $S_{n\pi^*}$ states (at low polarities) implies that the CIs, $(S_{\pi\pi^*}/S_{n\pi^*})_{CI}$ and also $(S_0/S_{n\pi^*})_{CI}$, are more accessible and, therefore, an increased rate constant is foreseen. On the other hand, as the $S_{\pi\pi^*}$ minimum deepens (smaller energy gap with S_0) in polar solvents, the decay rate becomes smaller because the $(S_{\pi\pi^*}/S_{n\pi^*})_{CI}$ becomes less accessible.

Regarding the ISC rate, our computed SOC values $S_{\pi\pi^*}/T_{n\pi^*}$ indicate that the ISC would be more favorable (11.1 cm^{-1}) at the $S_{\pi\pi^*}$ minimum, where the singlet–triplet crossing takes

place in nonpolar solvents and the energy gets trapped for a longer time, than closer to the initial geometry (4.3 cm^{-1}), that is, where the crossing occurs in polar environments. This type of mechanism for the population of the triplet manifold, in which the $T_{n\pi^*}$ intermediacy to populate the triplet manifold takes place along the spectroscopic singlet $S_{\pi\pi^*}$ relaxation path, is common in many organic systems (in particular for the important role of the SOC terms as controllers of the population transfer probability), and it has been described before in other molecules at the same level of calculation.^[25,38,42–45] Once in the lowest $T_{n\pi^*}$ state, the system is expected to decay to the lowest $T_{\pi\pi^*}$ state by IC within the triplet manifold (k_{TT}). The importance of other secondary channels cannot be ruled out.

For instance, we have also computed the excited states at the geometry of the $S_{n\pi^*}$ state, and there, $S_{n\pi^*}$ was found to be degenerated with the $2^3A \pi\pi^*$ state, with a large SOC term of 42.0 cm^{-1} . The population that reaches $S_{n\pi^*}$ by coupling with the lowest $S_{\pi\pi^*}$ state may then also give rise to efficient ISC toward the triplet manifold, with similar behavior against the solvent polarity because of the destabilization undergone by the $S_{n\pi^*}$ state. We should, in principle, consider this funnel less relevant in polar solvents. Consider

that the former discussion on the solvent dependence of the rate constants should be taken with care as it relies on an approximated calculation of the energy levels based on the Onsager model.

Obviously, the kinetics expressed in Equation (2) do not account for the nonequilibrium processes that the calculations suggest. These classical equations implicitly consider that all reactions take place between equilibrated states, which seems not always to be the case here. This may be the reason why our fits are not perfect. In other words, the details of the energy dissipation mechanism leading to the relaxed $S_{\pi\pi^*}$ state, coupled to IC and ISC processes, are not taken into account, and neither are the vibrational relaxation processes such as those responsible for the fluorescence band shrinking with time.^[46] To solve these issues is beyond the scope of the present work and would require an extensive experimental study of the early fluorescence dynamics over the whole emission spectrum of TX.

3. Conclusions

We have shown that the ultrafast photophysics of TX is governed by the IC and ISC processes from the spectroscopic $S_{\pi\pi^*}$ state toward the ground state and the lowest triplet $T_{n\pi^*}$ state, respectively, which take place through intermediate $n\pi^*$ -type states, $S_{n\pi^*}$ (IC) and $T_{n\pi^*}$ (ISC). The role of the $n\pi^*$ state in the

decay dynamics was earlier emphasized by suggesting TX as a paradigm for the occurrence of the proximity effect model. Large vibronic coupling between near-degenerate $\pi\pi^*$ and $n\pi^*$ states was supposed to lead to efficient decay toward the ground state via high-lying vibrational states of the latter.^[8] Here, TX photophysics is rationalized in terms of CIs and singlet–triplet crossings connecting the different states. In this respect, two CIs, easily accessible in the gas phase, connect the $S_{\pi\pi^*}$ and $S_{n\pi^*}$ states and the latter state with the ground state. Such a decay path is less accessible in polar solvents, hence explaining the measured decrease of the IC rate (and thus the increase of the quantum yield of fluorescence). This behavior is understandable if we consider the role of the $S_{n\pi^*}$ state as an intermediate, which is largely destabilized to higher energies in polar and protic solvents, and the strong stabilization of the $S_{\pi\pi^*}$ state, leading in both cases to the same outcome: the energy barriers to access the CIs increase and the IC is hindered. On the other hand, the ISC takes place closer to the FC configuration in polar solvents giving the system less time to evolve to the triplet state, and a similar behavior is expected as for the IC processes because in this case as well an $n\pi^*$ -type state acts as intermediate between the initial, $S_{\pi\pi^*}$, and final $T_{\pi\pi^*}$ states. The phenomenological classical kinetic scheme used to reproduce the experimental data, though leading to reasonably good results, has to be taken as merely indicative of the trends of the different processes changing with the solvent characteristics. Finally, this paper points out that TX photophysics is a real challenge for both experimentalists and theorists.

Acknowledgements

Financial support is acknowledged from projects CTQ2007-61260 and CSD2007-0010 Consolider-Ingenio in Molecular Nanoscience of the Spanish MEC/FEDER. This work was also supported by the Fonds National Suisse de la Recherche Scientifique through Project No. 200020-124392 and by the University of Geneva.

Keywords: ab initio calculations · conical intersections · photophysics · solvent effects · transition states

- [1] J. C. Dalton, F. C. Montgomery, *J. Am. Chem. Soc.* **1974**, *96*, 6230–6232.
 [2] a) T.-I. Lai, E. C. Lim, *Chem. Phys. Lett.* **1980**, *73*, 244–248; b) T.-I. Lai, E. C. Lim, *Chem. Phys. Lett.* **1981**, *84*, 303–307.
 [3] K. A. Abdullah, T. J. Kemp, *J. Photochem.* **1986**, *32*, 49–57.
 [4] D. Burget, P. Jacques, *J. Lumin.* **1992**, *54*, 177–181.
 [5] D. Burget, P. Jacques, *J. Chim. Phys.* **1991**, *88*, 675–688.
 [6] S. Ishijima, M. Higashi, H. Yamaguchi, *J. Phys. Chem.* **1994**, *98*, 10432–10435.
 [7] J.-P. Malval, B. Graff, P. Jacques, *EPA Newsl.* **2009**, 37.
 [8] a) W. A. Wassam, E. C. Lim, *J. Chem. Phys.* **1978**, *68*, 433–454; b) W. A. Wassam, E. C. Lim, *J. Chem. Phys.* **1978**, *69*, 2175–2180.
 [9] L. Serrano-Andrés, M. Merchán, A. C. Borin, *Proc. Natl. Acad. Sci. USA* **2006**, *103*, 8691–8696.
 [10] M. Klessinger, J. Michl, *Excited States and Photochemistry of Organic Molecules*, VCH, Weinheim, **1995**.
 [11] *Computational Photochemistry* (Ed.: M. Olivucci), Elsevier, Amsterdam, **2005**.
 [12] *Conical Intersections* (Eds.: W. Domke, D. R. Yarkony, H. Köppel), World Scientific, Singapore, **2004**.
 [13] X. Allonas, C. Ley, C. Bibaut, P. Jacques, J. P. Fouassier, *Chem. Phys. Lett.* **2000**, *322*, 483–490.
 [14] M. G. Neumann, M. H. Gehlen, M. V. Encinas, N. S. Allen, T. Corrales, C. Peinado, F. Catalina, *J. Chem. Soc. Faraday Trans.* **1997**, *93*, 1517–1521.
 [15] O. Rubio-Pons, L. Serrano-Andrés, D. Burget, P. Jacques, *J. Photochem. Photobiol. A* **2006**, *179*, 298–304.
 [16] C. Ley, F. Morlet-Savary, P. Jacques, J. P. Fouassier, *Chem. Phys.* **2000**, *255*, 335–346.
 [17] E. Krystkowiak, A. Maciejewski, J. Kubicki, *ChemPhysChem* **2006**, *7*, 597–606.
 [18] G. Duvanel, N. Banerji, E. Vauthey, *J. Phys. Chem. A* **2007**, *111*, 5361–5369.
 [19] S. Yamaguchi, H.-O. Hamaguchi, *Appl. Spectrosc.* **1995**, *49*, 1513–1515.
 [20] K. Andersson, P.-Å. Malmqvist, B. O. Roos, *J. Chem. Phys.* **1992**, *96*, 1218–1226.
 [21] P.-Å. Malmqvist, A. Rendell, B. O. Roos, *J. Phys. Chem.* **1990**, *94*, 5477–5482.
 [22] L. Serrano-Andrés, B. O. Roos, *Chem. Eur. J.* **1997**, *3*, 717–725.
 [23] O. Rubio-Pons, L. Serrano-Andrés, M. Merchán, *J. Phys. Chem. A* **2001**, *105*, 9664–9673.
 [24] P.-Å. Malmqvist, B. O. Roos, B. Schimmelpfennig, *Chem. Phys. Lett.* **2002**, *357*, 230–240.
 [25] M. Merchán, L. Serrano-Andrés, M. A. Robb, L. Blancafort, *J. Am. Chem. Soc.* **2005**, *127*, 1820–1825.
 [26] N. Forsberg, P.-Å. Malmqvist, *Chem. Phys. Lett.* **1997**, *274*, 196–204.
 [27] P.-O. Widmark, P.-Å. Malmqvist, B. O. Roos, *Theor. Chim. Acta* **1990**, *77*, 291–306.
 [28] G. Karlström, R. Lindh, P.-Å. Malmqvist, B. O. Roos, U. Ryde, V. Veryazov, P.-O. Widmark, M. Cossi, B. Schimmelpfennig, P. Neogrady, L. Seijo, *Comput. Mater. Sci.* **2003**, *28*, 222–239.
 [29] V. Veryazov, P.-O. Widmark, L. Serrano-Andrés, R. Lindh, B. O. Roos, *Int. J. Quantum Chem.* **2004**, *100*, 626–635.
 [30] L. Serrano-Andrés, J. Sánchez-Marín, I. Nebot-Gil, *J. Chem. Phys.* **1992**, *97*, 7499–7506.
 [31] L. Serrano-Andrés, M. Merchán, I. Nebot-Gil, R. Lindh, B. O. Roos, *J. Chem. Phys.* **1993**, *98*, 3151–3162.
 [32] B. O. Roos, M. P. Fülcher, P.-Å. Malmqvist, L. Serrano-Andrés, K. Pierloot, M. Merchán, *Adv. Chem. Phys.* **1996**, *93*, 219–331.
 [33] M. Merchán, R. González-Luque, T. Climent, L. Serrano-Andrés, E. Rodríguez, M. Reguero, D. Peláez, *J. Phys. Chem. B* **2006**, *110*, 26471–26476.
 [34] L. Serrano-Andrés, M. Merchán, A. C. Borin, *Chem. Eur. J.* **2006**, *12*, 6559–6571.
 [35] L. Serrano-Andrés, M. Merchán, A. C. Borin, *J. Am. Chem. Soc.* **2008**, *130*, 2473–2484.
 [36] Y. Marcus, *The Properties of Solvents*, Wiley, New York, **1998**.
 [37] L. Onsager, *J. Am. Chem. Soc.* **1936**, *58*, 1486–1493.
 [38] J. J. Serrano-Pérez, M. Merchán, L. Serrano-Andrés, *Chem. Phys. Lett.* **2007**, *434*, 107–110.
 [39] M. A. El-Sayed, *J. Chem. Phys.* **1963**, *38*, 2834–2838.
 [40] J. Tatchen, N. Gilka, C. M. Marian, *Phys. Chem. Chem. Phys.* **2007**, *9*, 5209–5221.
 [41] S. Perun, J. Tatchen, C. M. Marian, *ChemPhysChem* **2008**, *9*, 282–292.
 [42] T. Climent, R. González-Luque, M. Merchán, L. Serrano-Andrés, *J. Phys. Chem. A* **2006**, *110*, 13584–13590.
 [43] T. Climent, R. González-Luque, M. Merchán, L. Serrano-Andrés, *Chem. Phys. Lett.* **2007**, *441*, 327–331.
 [44] J. J. Serrano-Pérez, R. González-Luque, M. Merchán, L. Serrano-Andrés, *J. Phys. Chem. B* **2007**, *111*, 11880–11883.
 [45] J. J. Serrano-Pérez, R. González-Luque, M. Merchán, L. Serrano-Andrés, *J. Photochem. Photobiol. A* **2008**, *199*, 34–41.
 [46] A. Pigiucci, G. Duvanel, L. M. L. Daku, E. Vauthey, *J. Phys. Chem. A* **2007**, *111*, 6135–6145.

Received: August 18, 2009

Published online on January 12, 2010